Supplementary Material

Newly identified climatically and environmentally significant high-latitude dust sources

Outi Meinander[1], Pavla Dagsson-Waldhauserová[2,3], Pavel Amosov[4], Elena Aseyeva[5], Cliff Atkins[6], Alexander Baklanov[7], Clarissa Baldo[8], Sarah Barr[9], Barbara Barzycka[10], Liane G. Benning[11,23], Bojan Cvetkovic[12], Polina Enchilik[5], Denis Frolov[5], Santiago Gassó[13], Konrad Kandler[14], Nikolay Kasimov[5], Jan Kavan[15], James King[16], Tatyana Koroleva[5], Viktoria Krupskaya[5,6], Markku Kulmala[18], Monika Kusiak[19], Hanna K Lappalainen[18], Michał Laska[11], Jerome Lasne[20], Marek Lewandowski[19], Bartłomiej Luks[19], James B McQuaid[10], Beatrice Moroni[21], Benjamin J Murray[10], Ottmar Möhler[22], Adam Nawrot[19], Slobodan Nickovic[13], Norman T. O'Neill[23], Goran Pejanovic[13], Olga B. Popovicheva[5], Keyvan Ranjbar[23,a], Manolis N. Romanias[20], Olga Samonova[5], Alberto Sanchez-Marroquin[10], Kerstin Schepanski[24], Ivan Semenkov[5], Anna Sharapova[11], Elena Shevnina[1], Zongbo Shi[9], Mikhail Sofiev[1], Frédéric Thevenet[20], Throstur Thorsteinsson[25], Mikhail A. Timofeev[5], Nsikanabasi Silas Umo[22], Andreas Uppstu[1], Darya Urupina[20], György Varga[26], Tomasz Werner[19], Olafur Arnalds[2], and Ana Vukovic Vimic[27]

[1]Finnish Meteorological Institute, Helsinki, 00101, Finland
[2]Agricultural University of Iceland, Reykjavik, 112, Iceland
[3]Czech University of Life Sciences Prague, Prague, 16521, Czech Republic
[4]INEP Kola Science Center RAS, Apatity, Russia
[5]Lomonosov Moscow State University, Moscow, 119991, Russia
[6]Institute of Geology of Ore Deposits, Petrography, Moscow, 119017, Russia
[7]Te Herenga Waka—Victoria University of Wellington, Wellington, 6012, New Zealand
[87]World Meteorological Organization, WMO, Geneva, 1211, Switzerland
[9]University of Birmingham, Birmingham, B15 2TT, United Kingdom
[10]University of Leeds, Leeds, LS2 9JT, United Kingdom
[11]University of Silesia in Katowice, Sosnowiec, 41-200, Poland
[12]German Research Centre for Geosciences, Helmholtz Centre Potsdam, 14473, Germany
[13]Republic Hydrometereological Service of Serbia, 11030, Belgrade, Serbia
[14]University of Maryland, College Park MD, 20742, United States of America
[15]Technical University of Darmstadt, Darmstadt, 64287, Germany
[16]Masaryk University, Brno, 61137, Czech Republic
[17]University of Montreal, Montreal, H3T 1J4, Canada
[18]Institute for Atmospheric and Earth System Research, University of Helsinki, Helsinki, 00101, Finland
[19]Institute of Geophysics, Polish Academy of Sciences, Warsaw, 01-452, Poland
[20]IMT Lille Douai, SAGE, Université de Lille, 59000 Lille, France
[21]University of Perugia, Perugia, 06123, Italy
[22] Institute of Meteorology and Climate Research, Karlsruhe Institute of Technology, Karlsruhe, 76227, Germany.
[23]Université de Sherbrooke, Sherbrooke, J1K, Canada

[24]Free University of Berlin, Berlin, 12165, Germany
[25]University of Iceland, Reykjavik, 102, Iceland
[26]Research Centre for Astronomy and Earth Sciences, Budapest, 1112, Hungary
[27]University of Belgrade, Faculty of Agriculture, Belgrade, 11080, Serbia
[a]now at: Flight Research Laboratory, National Research Council Canada, Ottawa, ON, Canada

Supplementary Animation

http://www.seevccc.rs/HLDpaper/NMMB_DREAM_circumpolar_dustload_animation.gif

Supplementary Tables and Figures

Table S1. The contemporary category of the newly identified high-latitude dust sources included in this study based on the currently available observations. The number refers to the source number of the map in Figure 1. Also, McMurdo Dry Valley is estimated to best fit Category 3 and the McMurdo Ice Shelf 'debris bands' to Category 2.

Cat	HLD No.	Description	Climatic or environmental significance	Criteria
1	30, 31, 32, 34	Active source	High	Frequently active dust source with >10 dust events documented
2	25, 26, 27, 35	Moderately active source	Moderate	5–10 dust events documented or a smaller potential source area
3	1, 2-24, 28-29, 33, 36 –64	Source with unknown activity	Small/Currently unknown	Infrequent activity or a new source with 1–5 dust events documented

Table S2. Iceland dust sources and observations on dust events identified in this study based on satellite images of 2002–2011, source numbers 23–35 in Figure 1.

Location in Iceland	Satellite observations

No. 23 Reykjanes	2 events, 2004 and 2011
No. 24 Eyrabakki	3 events, 2002–2011
No. 25 Hagavatnssvæði	8 events, 2002–2011
No. 26 Fljótshlíð	8 events, 2002–2011
No. 27 Langisjór	5 events in 2010; 3 events in 2002–2011
No. 28 Eldhraun/Landbrot	3 events 2002–2011
No. 29 Eldhraun	3 events 2002–2011
No. 30 Klausturfjara	17 events 2002–2011
No. 31 Núpsvötn	39 events 2002–2011
No. 32 Holuhraun	29 events 2002–2011
No. 33 Vikurhraun/Vikursandur	2 events 2002–2011
No. 34 Höfn í Hornarfirði	13 events 2002–2011
No. 35 Lónsvík	8 events 2002–2011

Table S3. West coast of Greenland observations for the new dust sources identified for the first time in this study (No. 53–58 in Fig. 1), based on satellite observations from 2021 and earlier satellite observations for sources identified in East Greenland and Canada (No. 59–64), north of 70ºN

Latitude	Longitude	No.	Description	Dust example	Observed events
63.5059	-51.0454	53	West coast of Greenland, the source appears to be in the delta area, not in the valley	https://go.nasa.gov/3biOSt9	26 Oct 2021
62.2421	-49.0481	54	West coast of Greenland, the source appears to be a	https://go.nasa.gov/3Gw80SV	23/25 Oct 2021

			small valley with a glacier		
63.5163	-50.9652	55	West coast of Greenland, source appears to be the delta area (Sentinel shows dust plumes up 10 km from the coast, east of delta)	https://go.nasa.gov/3Ct5cmY	18,19,25,26 Oct 2021
65.7621	-51.2866	56	West coast of Greenland, a very narrow valley (not clear if dust comes from the valley or termination tip of glacier). Clear dust plumes when flipping images Aqua/Terra	https://go.nasa.gov/2ZBLvv2	18 and 22 Oct 2021
62.4791	-50.2146	57	West coast of Greenland, small trip of land between sea and glacier	https://go.nasa.gov/2ZyWbea	18 Oct 2021
67.359	-52.3693	58	West coast of Greenland, a short valley, several dust clouds appear	https://go.nasa.gov/3vU4qwR	18 Oct 2021
71.8288	-22.8017	59	East Greenland	https://go.nasa.gov/3pOPjnq	3 Oct 2019
70.4565	-22.2694	60	East Greenland	https://go.nasa.gov/3Gx1paM	15 Sep 2020
78.0407	-21.4572	61	East Greenland	https://go.nasa.gov/3Gw4g3R	24 Sep 2003
81.3073	-78.2145	62	Canada	https://go.nasa.gov/3mxJxEZ	2 July 2020
71.8426	-22.7902	63	East Greenland, better seen in S2 and L8	https://go.nasa.gov/3Bt9jy2	30 Sept 2018
72.3906	-25.1555	64	East Greenland	https://go.nasa.gov/3vXOWb6	23 Sep 2003

Table S4. Locations of the HLD sources (no. 1-64 in Fig. 1) and G-SDS-SBM source intensity (SI) values at location; maximum values found in certain environments given location (areas within the distance from location of 30 arcsec, 0.1°, 0.5°, and 1°); SI is undefined (-99.0) if location mark is not over land; area south of 60°S is not included in G-SDS-SBM, and values at locations in this area are marked with a dash.

No.	**lat**	**lon**	**at loc.**		**30 arcsec**		**0.1°**		**0.5°**		**1°**	
			max	**min**	**max**	**min**	**max**	**min**	**max**	**min**	**max**	**min**
1	57.6482	10.4059	0.8	0.0	0.9	0.0	1.0	0.0	1.0	1.0	1.0	1.0
2	63.2	75.5	0.1	0.0	0.1	0.0	0.1	0.0	0.3	0.2	0.5	0.2

3	60.1	71.4	0.0	0.0	0.0	0.0	0.3	0.0	0.3	0.0	0.8	0.3
4	58.9	69.2	0.0	0.0	0.0	0.0	0.2	0.0	0.7	0.3	0.8	0.3
5	56.5	67.5	0.1	0.0	0.2	0.0	0.2	0.0	0.3	0.1	0.5	0.1
6	67.6	33.4	0.0	0.0	0.0	0.0	0.8	0.0	0.9	0.0	1.0	0.0
7	51.3	88.5	0.0	0.0	0.0	0.0	0.2	0.0	0.4	0.0	0.4	0.2
8	47.3	66.7	0.5	0.0	0.5	0.0	0.6	0.3	0.7	0.4	1.0	0.7
9	-77.9	165.2	-	-	-	-	-	-	-	-	-	-
10	63.5	-18.2	1.0	0.0	1.0	0.0	1.0	1.0	1.0	1.0	1.0	1.0
11	71.4	128.5	0.0	0.0	0.3	0.0	0.4	0.0	1.0	0.0	1.0	0.0
12	81.7	-71.1	0.7	0.0	0.8	0.0	1.0	0.0	1.0	0.0	1.0	0.0
13	77	16	-99.0	-99.0	-99.0	-99.0	0.9	0.0	1.0	0.0	1.0	0.0
14	60.5	-144.9	0.6	0.0	0.9	0.0	1.0	0.0	1.0	0.5	1.0	0.5
15	56.0054	8.1138	0.0	0.0	0.9	0.0	1.0	0.0	1.0	1.0	1.0	1.0
16	69.36	-123.97	0.7	0.0	1.0	0.0	1.0	0.0	1.0	0.0	1.0	0.0
17	-45.48	-68.78	0.0	0.0	0.7	0.7	0.8	0.7	0.9	0.8	0.9	0.8
18	77	15	-99.0	-99.0	-99.0	-99.0	1.0	0.0	1.0	0.0	1.0	0.0
19	-63.9	-57.9	-	-	-	-	-	-	-	-	-	-
20	-64.2	-56.6	-	-	-	-	-	-	-	-	-	-
21	70.4	-52.5	0.5	0.0	0.6	0.0	0.8	0.0	1.0	0.0	1.0	0.0
22	78.7	15.7	0.3	0.0	0.3	0.0	0.7	0.0	1.0	0.0	1.0	0.0
23	63.85	-22.21635	0.0	0.0	0.7	0.1	1.0	0.9	1.0	1.0	1.0	1.0
24	63.87	-21.18885	0.0	0.0	1.0	0.0	1.0	0.0	1.0	1.0	1.0	1.0
25	64.47	-20.32702	0.4	0.0	0.4	0.0	0.6	0.2	0.8	0.5	1.0	1.0
26	63.72	-20.14013	0.2	0.0	0.2	0.0	0.3	0.1	1.0	1.0	1.0	1.0
27	64.14	-18.29022	0.3	0.0	0.3	0.0	0.4	0.0	0.9	0.7	1.0	1.0
28	63.69	-18.20012	0.0	0.0	0.4	0.0	1.0	1.0	1.0	1.0	1.0	1.0
29	64.03	-17.99276	0.0	0.0	0.2	0.0	0.3	0.0	1.0	1.0	1.0	1.0

30	63.7	-17.7592	0.9	0.0	0.9	0.0	1.0	0.7	1.0	1.0	1.0	1.0
31	63.91	-17.5464	0.6	0.0	0.6	0.5	1.0	0.5	1.0	1.0	1.0	1.0
32	64.84	-16.8455	0.2	0.0	0.3	0.0	0.5	0.0	0.5	0.0	1.0	1.0
33	65.02	-16.4949	0.0	0.0	0.2	0.0	0.5	0.0	0.6	0.3	1.0	1.0
34	64.24	-15.2144	0.0	0.0	0.0	0.0	1.0	0.1	1.0	1.0	1.0	1.0
35	64.38	-14.7674	0.3	0.0	0.7	0.0	1.0	1.0	1.0	1.0	1.0	1.0
36	-45.56	-68.7378	0.0	0.0	0.7	0.6	0.8	0.7	0.9	0.8	0.9	0.9
37	-53.217	-68.6934	0.0	0.0	0.3	0.2	1.0	0.9	1.0	1.0	1.0	1.0
38	-53.78	-67.8064	0.9	0.0	1.0	0.0	1.0	0.9	1.0	1.0	1.0	1.0
39	-49.53	-68.1744	0.9	0.9	0.9	0.9	1.0	1.0	1.0	1.0	1.0	1.0
40	-47.61	-65.7979	1.0	1.0	1.0	1.0	1.0	1.0	1.0	1.0	1.0	1.0
41	-47.94	-66.2073	0.8	0.7	0.8	0.7	1.0	1.0	1.0	1.0	1.0	1.0
42	-46.72	-69.0699	0.8	0.7	0.8	0.7	0.9	0.8	0.9	0.8	0.9	0.9
43	-46.53	-69.401	0.7	0.7	0.7	0.7	0.7	0.7	0.9	0.9	0.9	0.9
44	-48.54	-67.015	0.8	0.8	0.8	0.8	1.0	1.0	1.0	1.0	1.0	1.0
45	-41.14	-69.46	0.0	0.0	0.5	0.3	0.6	0.4	0.6	0.5	0.8	0.5
46	70.47	-52.88	0.5	0.0	0.9	0.0	0.9	0.0	1.0	0.0	1.0	0.0
47	71.36	-24.53	0.6	0.0	0.6	0.0	1.0	0.0	1.0	0.0	1.0	0.0
48	47.6	-111.25	0.5	0.1	0.8	0.1	0.8	0.7	1.0	0.7	1.0	0.9
49	67.87	44.13	1.0	0.0	1.0	0.0	1.0	0.0	1.0	0.0	1.0	0.0
50	60.9987	-138.529	0.6	0.0	0.7	0.3	0.7	0.3	0.9	0.5	1.0	0.6
51	56.4772	12.9260	0.0	0.0	0.0	0.0	0.9	0.0	1.0	0.6	1.0	0.6
52	-70.7583	11.6444	-	-	-	-	-	-	-	-	-	-
53	63.5059	-51.0454	0.0	0.0	0.5	0.0	1.0	0.2	1.0	1.0	1.0	1.0
54	62.2421	-49.0481	0.4	0.0	0.5	0.0	0.8	0.3	1.0	1.0	1.0	1.0
55	63.5163	-50.9652	0.0	0.0	0.5	0.0	1.0	0.2	1.0	1.0	1.0	1.0

56	65.7621	-51.2866	0.0	0.0	0.6	0.0	0.9	0.0	0.9	0.0	1.0	1.0
57	62.4791	-50.2146	0.5	0.0	0.6	0.0	0.6	0.3	1.0	0.9	1.0	1.0
58	67.359	-52.3693	0.4	0.0	0.5	0.0	1.0	0.0	1.0	0.1	1.0	1.0
59	71.8288	-22.8017	0.0	0.0	1.0	0.0	1.0	0.0	1.0	0.0	1.0	0.0
60	70.4565	-22.2694	0.9	0.0	1.0	0.0	1.0	0.0	1.0	0.0	1.0	0.0
61	78.0407	-21.4572	1.0	0.0	1.0	0.0	1.0	0.0	1.0	0.0	1.0	0.0
62	81.3073	-78.2145	0.0	0.0	0.0	0.0	0.0	0.0	0.9	0.0	1.0	0.0
63	71.8426	-22.7902	0.0	0.0	0.0	0.0	1.0	0.0	1.0	0.0	1.0	0.0
64	72.3906	-25.1555	-99.0	-99.0	-99.0	-99.0	0.3	0.0	0.4	0.0	1.0	0.0

Table S5. Number of locations for north and south HLD regions that have SI values above a certain threshold (0.9, 0.8, 0.7, 0.6, 0.5, 0.4), depending on the environment size (30 arcsec, 0.1°, 0.5°, and 1°)

No.	lat	lon	at loc.		30 arcsec		0.1°		0.5°		1°	
			max	min	max	min	max	min	max	min	max	min
NORTH HLD REGION (NORTH OF 50°N)												
SI ≥ 0.9			5	0	12	0	27	4	39	16	44	23
SI ≥ 0.8			6	0	14	0	31	4	40	16	46	23
SI ≥ 0.7			8	0	17	0	33	6	42	18	46	24
SI ≥ 0.6			12	0	22	0	36	6	43	19	46	26
SI ≥ 0.5			17	0	27	1	38	7	44	22	48	27
SI ≥ 0.4			20	0	29	1	40	7	46	23	49	27
SOUTH HLD REGION (SOUTH OF 40°S)												
SI ≥ 0.9			3	2	3	2	7	6	10	7	10	9
SI ≥ 0.8			6	3	6	3	9	7	10	10	11	10
SI ≥ 0.7			7	6	9	7	10	10	10	10	11	10
SI ≥ 0.6			7	6	9	8	11	10	11	10	11	10
SI ≥ 0.5			7	6	10	8	11	10	11	11	11	11
SI ≥ 0.4			7	6	10	8	11	11	11	11	11	11

Table S6. Mineralogical and elemental composition of PM2 and PM1000 of soils in Western Siberia.

Proxy	HLD no.2 (Podzols)			HLD no.3 (Retisols and Gleysols)				HLD no.4 (Retisols and Gleysols)				HLD no.5 (Phaeozems and Stagnosols)			
	PM2, n=1	PM1000, n=10		PM2, n=4		PM1000, n=7		PM2, n=5		PM1000, n=5		PM2, n=8		PM1000, n=11	
	M	M	σ	M	σ	M	σ	M	σ	M	σ	M	σ	M	σ
Smectite, %	36.7	0.0	0.0	51.5	4.1	13.7	10.4	46.8	5.5	17.7	10.5	47.6	11.6	23.2	8.7
Illite, %	5.5	2.9	1.0	8.7	1.4	9.3	0.8	8.1	0.9	6.3	0.7	8.3	2.2	10.1	1.5
I/Sm, %	23.6	<0.1	-	18.2	1.0	<0.1	-	20.1	5.1	<0.1	-	26.0	10.1	<0.1	-
Kaolinite, %	6.7	1.4	1.2	3.5	0.8	2.3	0.6	6.5	2.5	2.2	1.1	5.3	1.7	3.4	0.7
Chlorite, %	2.1	0.4	0.5	2.4	0.8	1.0	0.7	1.1	1.1	2.1	0.8	1.9	0.5	1.7	0.7
Pls, %	6.4	5.5	2.7	4.3	0.8	15.5	3.2	4.5	0.7	14.6	3.4	3.5	1.3	13.8	2.5
PFS, %	7.1	4.9	3.0	4.9	1.3	8.3	1.9	4.3	0.9	8.3	1.4	5.4	1.8	8.1	1.6
Quartz, %	11.2	84.6	6.8	5.7	1.7	49.8	10.2	7.6	4.5	48.7	8.9	4.1	2.6	38.4	6.2
Calcite, %	0.8	0.4	0.2	1.1	0.2	0.0	0.0	1.0	0.7	0.0	0.0	2.0	2.6	1.4	3.1
TOC, %	n.a.	1.7	3.7	1.0	1.0	4.7	7.3	6.0	4.3	1.8	2.9	2.4	3.1	1.0	1.4
Na_2O, %	0.71	0.54	0.32	0.25	0.14	0.99	0.33	0.19	0.09	1.23	0.26	0.18	0.05	0.87	0.24
MgO, %	1.14	0.13	0.11	1.97	0.22	1.18	0.67	1.73	0.37	1.28	0.29	2.33	0.29	1.75	0.43
Al_2O_3, %	20.7	3.5	2.0	15.6	3.1	10.9	2.8	16.2	2.7	10.9	1.3	17.2	3.3	12.0	1.9
P_2O_5, %	0.34	0.47	0.47	0.34	0.47	0.13	0.07	0.44	0.26	0.16	0.15	0.25	0.21	0.27	0.41
S, %	0.24	0.04	0.02	0.14	0.25	0.09	0.04	0.12	0.15	<0.1	-	0.06	0.07	0.06	0.02
K_2O, %	1.64	1.18	0.54	1.86	0.32	1.74	0.29	1.59	0.17	1.88	0.16	2.50	0.42	2.14	0.26
CaO, %	0.48	0.16	0.07	1.20	0.34	0.75	0.36	1.05	0.47	1.18	0.36	2.32	1.77	1.97	2.00

TiO_2, %	0.92	0.33	0.19	0.71	0.14	1.03	0.04	0.61	0.14	1.00	0.21	0.62	0.11	0.97	0.08
MnO, %	0.29	0.02	0.01	0.10	0.06	0.06	0.04	0.13	0.08	0.10	0.09	0.07	0.04	0.12	0.08
Fe_2O_3, %	9.1	0.5	0.4	8.8	2.2	3.6	2.0	9.2	2.8	4.9	1.2	8.8	1.1	5.3	1.5
V, mg/kg	171	30	17	174	45	123	24	164	35	115	14	168	24	140	16
Cr, mg/kg	754	36	26	298	251	129	20	231	67	144	16	216	96	154	28
Co, mg/kg	62	<10	-	22	4.4	15.3	3.5	26.2	6.4	20	7.5	17	2.1	17	3.8
Ni, mg/kg	182	<10	-	115	45	29	15	85	8.0	32	9.4	90	25	47	11
Cu, mg/kg	59	<10	-	54	5.0	20	5.3	38	10	15	1.5	48	9.9	28	4.5
Zn, mg/kg	180	26	8.1	144	21	50	22	136	25	61	17	126	9.7	75	12
As, mg/kg	15	<10	-	13	2,4	<10	-	14	4.5	<10	-	12	3.2	<10	-
Pb, mg/kg	36	<10	-	32	21	19	5.3	28	7.1	23.3	12	19	3.3	27	5.1

I/Sm – illite-smectite mixed-layer minerals with predomination of illite interlayers, PLs – Plagioclases PFS – potassium feldspars, TOC – total organic carbon

Table S7. Some characteristics of tailing ponds on the Kola Peninsula (Masloboev et al., 2016).

No.	Object	Exploitation period	Total area, ha	Resource, mln. t
1	Tailing pond of processing plant no. 1 of the Pechenganickel works, JSC Kola MMC	1945–1994	1033	~220
2	Tailing pond of processing plant no. 2 of the Pechenganickel works, JSC Kola MMC	1965– present time		22.4
3	Tailing pond of processing plant of the Severonikel works, JSC Kola MMC	1935–1978	No data	5.3
4	Dumps of granulated slag of the Pechenganickel works, JSC Kola MMC	1945– present time	80	47
5	Tailing pond no. 1 and no. 2 of crushing and processing plant, JSC Olkon	1954– present time	1400	~300
6	Tailing pond of apatite-nepheline processing plant no.1 (ANOF-1), JSC Apatit	1957–1963	120	24.4
7	Tailing pond of apatite-nepheline processing plant no. 2 (ANOF-2), JSC Apatit	1963– present time	1652	~550
8	Tailing pond of apatite-nepheline processing plant no. 3 (ANOF-3), JSC Apatit	1988– present time	1158	~250
9	Tailing pond of JSC Kovdorskiy GOK, (field no. 1)	1962–1980	330	53.8
10	Tailing pond of JSC Kovdorskiy GOK, (field no. 2)	1988– present time	900	80
11	Tailing pond of LLC Lovoserskiy GOK	1951– present time	No data	12
12	Tailing pond of LLC Kovdorslyuda	1959 – present	35	6

Supplement: Central part of the East European Plain: partitioning of chemical elements among five particle-sized fractions

Topsoil (0–10 cm) samples were collected along several transects (Samonova and Aseyeva, 2020), crossing two small erosional landforms—a gully and a balka (Fig 1A). The collected bulk samples (n=22) were physically fractionated into five particle-sized fractions (250–1000, 50–250, 10–50, 1–10, and <1 μm, n=100). The boundaries among particle size classes were defined according to the Russian conventional fraction groups: coarse and medium sand (250–1000 μm), fine sand (50–250 μm), coarse silt (10–50 μm), medium and fine silt (1–10 μm), and clay (<1 μm). The concentrations of Al, Fe, Mn, Ti, Li, Be, Sc, V, Cr, Co, Ni, Cu, Zn, Ga, As, Rb, Mo, Cd, Sn, Sb, Cs, Pb, Ta, Tl, Bi, Th, Y, Nb, Ba, U, Zr, Sr, and Hf were determined on Elan-6100 and Optima-4300 DV spectrometers (Perkin Elmer Inc., USA) by ICP-AES/MS after the samples were digested in a mixture of acids (NSAM-499-AES/MS method). In physical fractionation, the sand fractions were separated from the bulk soil samples by wet sieving, while the silt and clay fractions were obtained by sedimentation and siphoning during times determined by Stokes' law.

The measured concentrations and element distribution among soil particle-sized fractions are shown in Figs. 2A, 3A, and 4A. Because of the different ways in which the elements can occur in the soils (Samonova and Aseyeva, 2020), their distribution among particle-sized fractions varies. However, some common patterns in partitioning the elements exist, which allowed us to combine them into several distinct groups (groups A, B, and C). According to our results, most of the elements (Al, Cd, Zn, Sc, V, Tl, Pb, Rb, Ti, Nb, Th, Y, U, Li, Cs, Be, and Ga) showed the progressive accumulation from the coarser to the finer fractions and a maximum of the element concentration in the clay fraction (Fig.2A). The predominant accumulation of metals in the fine fractions was reported earlier for the natural and polluted soils (Hardy and Cornu, 2006; Ljung et al., 2006), suggesting these elements are mainly found in the secondary minerals such as phyllosilicate clays, where they occur as structural components or adsorbed ions. A more detailed study of the element partitioning showed that group A was not homogeneous because of some differences in the distribution of the elements between the two sand fractions, which allowed us to identify several subgroups of the elements. The first subgroup (Al, Cd, Zn, Sc, V, Tl, Pb, and Rb) included the elements partitioned equally between the two sand fractions. The second contained Ti, Nb, Th, Y, and U, with higher affinity to the finer sand fraction, presumably due to the preferential accumulation of stable minerals like rutile and titanite in the fine sand and silt fractions. The third included the lithophile elements (Li, Cs, Be, Ga) associated more closely with the coarser sand fraction than the fine sand fraction.

Unlike group A, the elements from group B had minimal concentrations, not in the sand but the silt fractions, specifically the coarse silt fraction (Cr, Ni, Sn, Bi, Sb, As, Mn, and Co) or both silt fractions (Fe and Mo). However, the major element hosting a particle-sized fraction remained the same (the clay fraction). Most of the elements comprising this group participate in redox reactions and belong to the arsenic group or represent typical elements of the ferro-family. The latter group can occur in soils as structural components of primary ferrous minerals or/and as co-precipitates in secondary Fe-Mn (hydr)oxides. Most of the elements from group B did not concentrate in the sand fractions, except for Mn, Co, and Mo, which, in some cases, displayed

two concentration maxima (one in clay and one in sand). Such bimodal distribution was reported earlier and can be explained by the presence of several hosting minerals and phases having high retention for these metals. In the clay, Mn and Co are associated with secondary clay minerals. However, in the sand, they seem bound to newly formed Mn (hydr)oxides.

The last group (group C) incorporated stable elements Zr and Hf. Their maximum concentrations were observed in the silt fractions, with a maximum in the coarse silt and a minimum in the coarse and medium sand fractions. Such distribution among different particle-sized fractions can be explained by the occurrence of these elements in detrital grains of primary accessory minerals, such as zircon, usually concentrated in the fine sand to coarse silt fractions.

In conclusion, our geochemical study conducted in the central part of European Russia showed that most of the elements in the upper horizons of typical silty soils displayed progressive accumulation in the finer fractions. However, our data also proves that the preferential association of the elements with particle-sized fractions is not limited to the clay fraction. Metals such as Mn and Co tend to have bimodal distribution with concentration maxima in the clay and sand fractions. The partitioning of Zr, Hf, Nb, Ti, U, and Y accumulating in the silt fractions is governed by their presence in the mineral structure of accessory minerals that are stable during transport, physicochemical weathering, and soil formation. In many cases, the coarse silt fraction, with particle sizes of 10–50 μm, is depleted in elements, which can stem from its loessial origin.

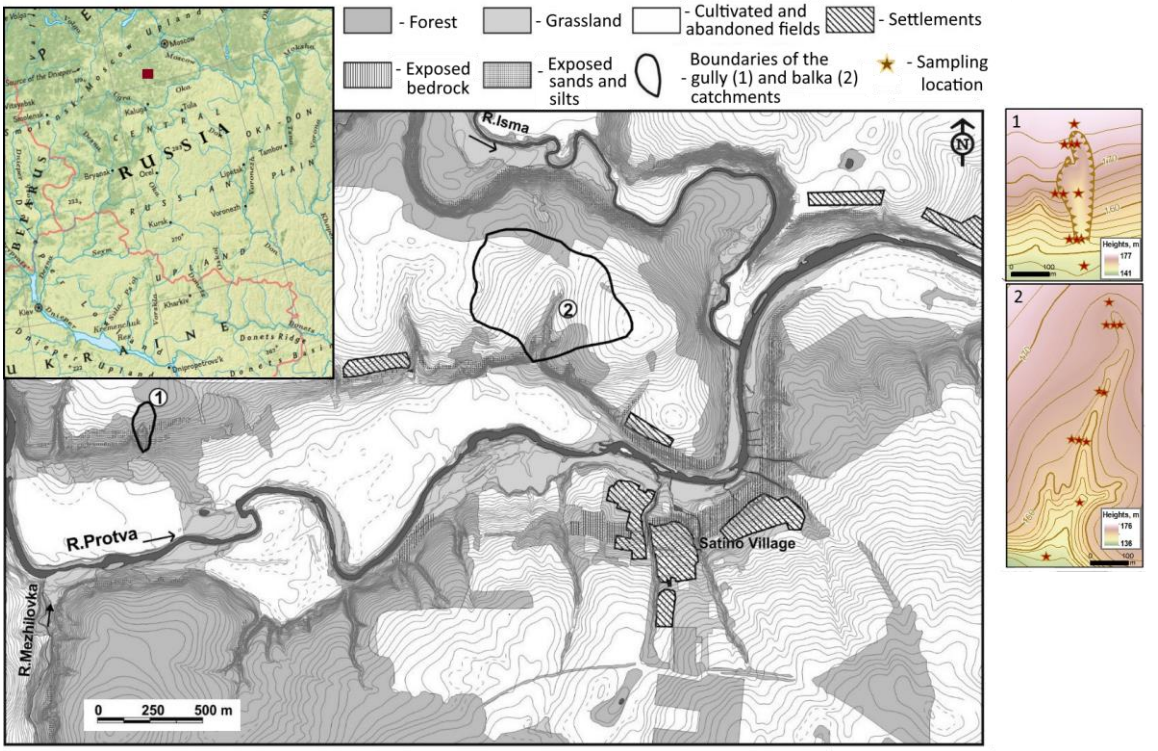

Figure S1. Map of the study area in Central European Russia with the study objects and sampling locations (Samonova and Aseyeva, 2020).

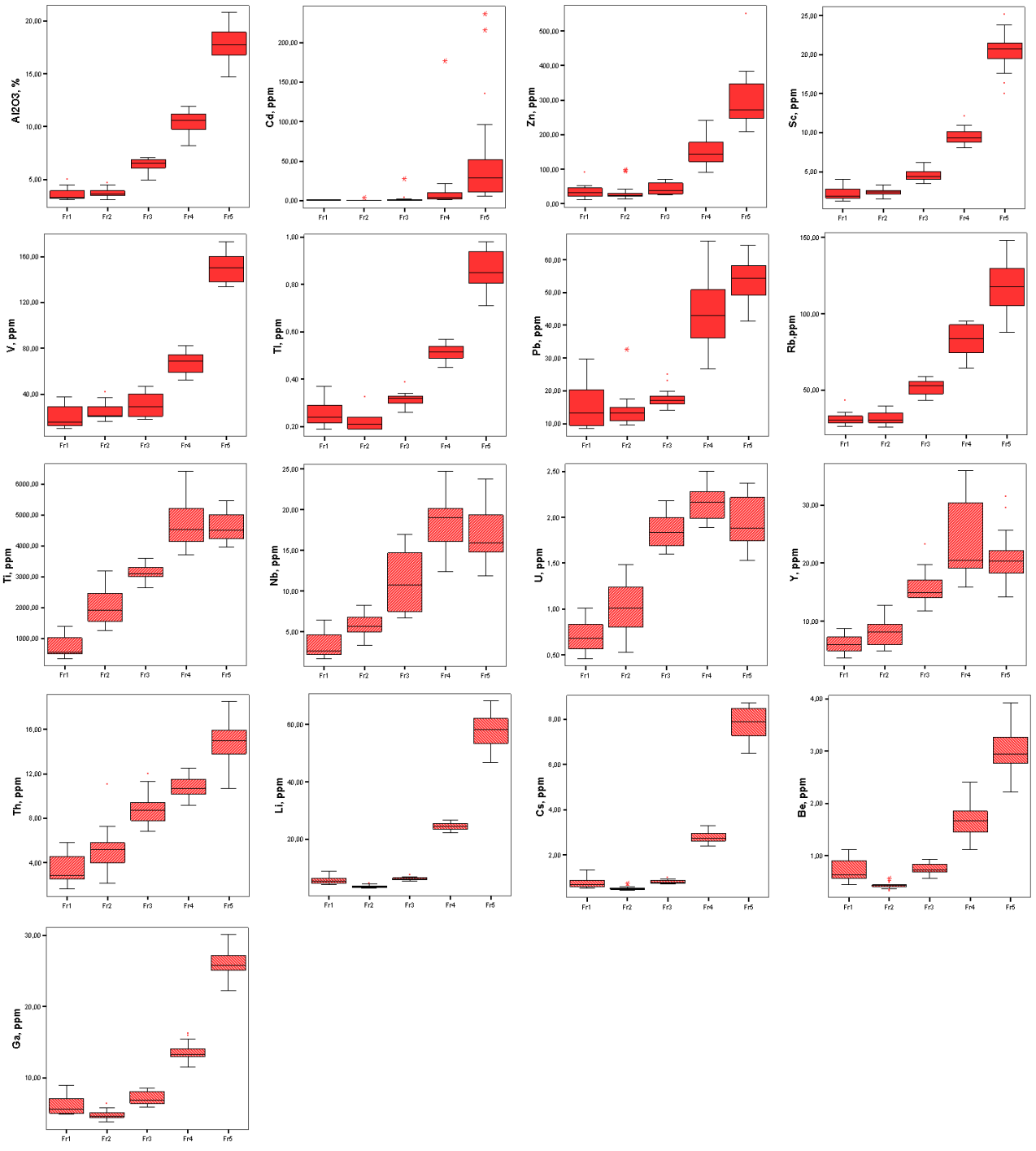

Figure S2. The abundances of elements (group A) in the soil particle size fractions. Median is indicated as a line across the box. X-axe: particle size fractions Fr1 – coarse and medium sand (250–1000 μm); Fr2 – fine sand (50–250 μm); Fr3 – coarse silt (10–50 μm); Fr4 – medium and fine silt (1–10 μm); Fr5 – clay (<1 μm).

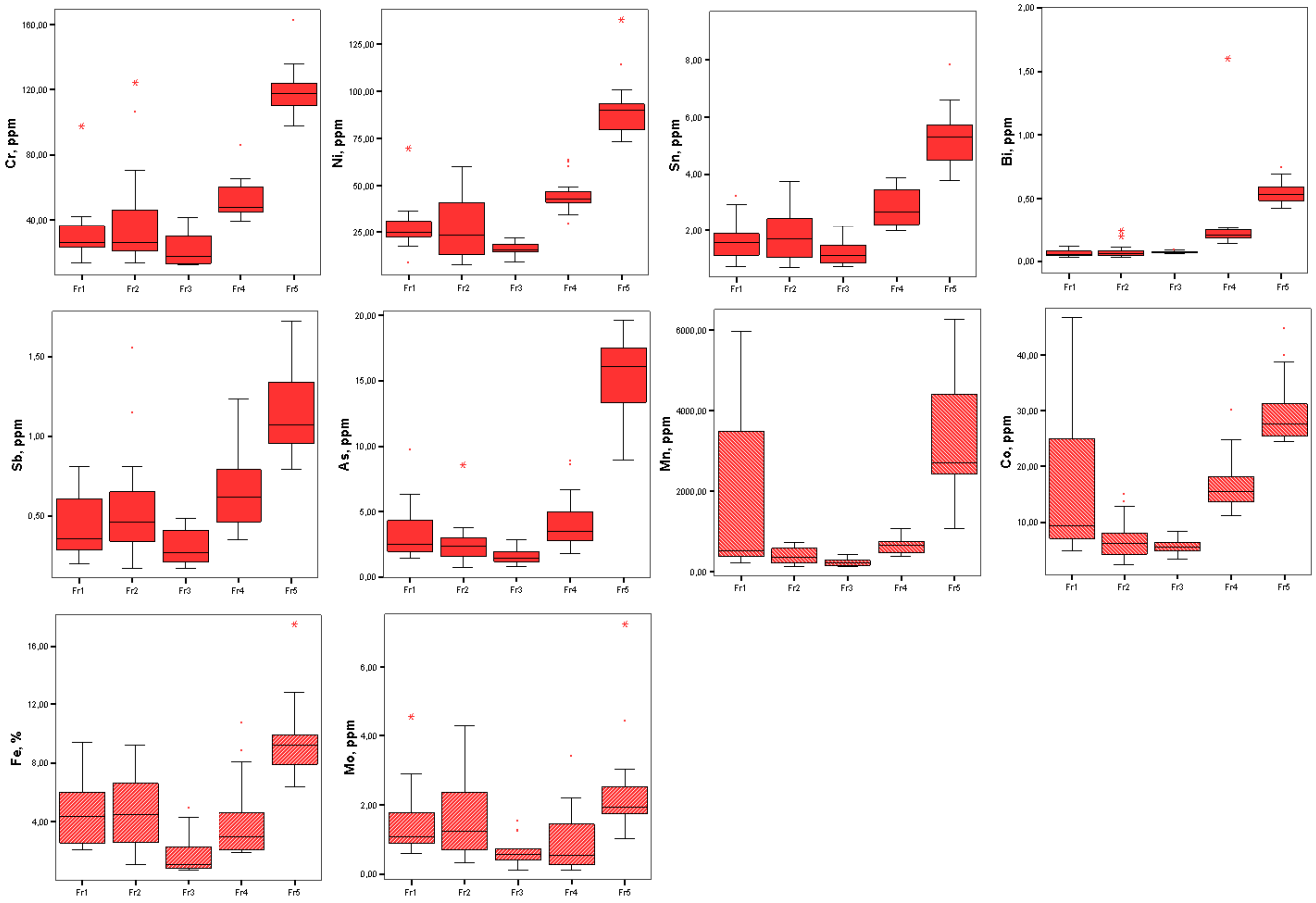

Figure S3. The abundances of elements (group B) in the soil particle size fractions. Median is indicated as a line across the box. X-axe: particle size fractions Fr1 – coarse and medium sand (250–1000 μm); Fr2 – fine sand (50–250 μm); Fr3 – coarse silt (10–50 μm); Fr4 – medium and fine silt (1–10 μm); Fr5 – clay (<1 μm).

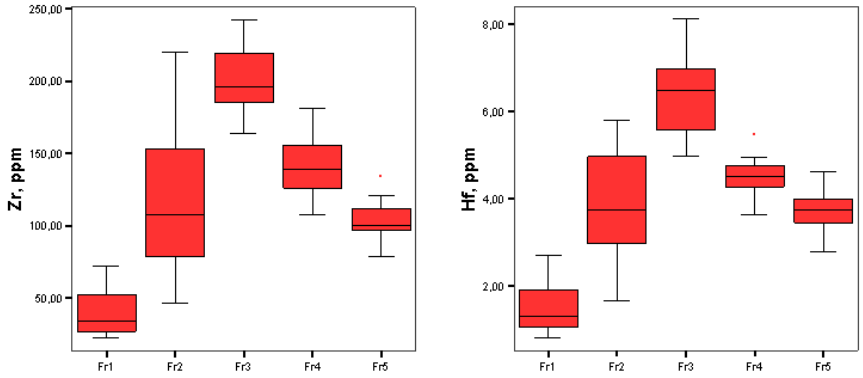

157

158

159 **Figure S4. The abundances of elements (group C) in the soil particle size fractions.** Median is indicated as a line across the box. X-axe:
160 particle size fractions Fr1 – coarse and medium sand (250–1000 μm); Fr2 – fine sand (50–250 μm); Fr3 – coarse silt (10–50 μm); Fr4 –
161 medium and fine silt (1–10 μm); Fr5 – clay (<1 μm).

162

163